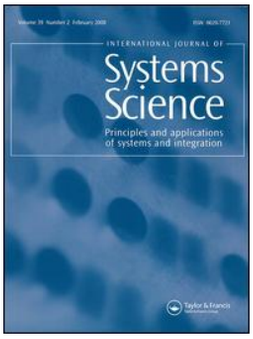

International Journal of Systems Science

ISSN: (Print) (Online) Journal homepage: https://www.tandfonline.com/loi/tsys20

Adaptive PID-fractional-order nonsingular terminal sliding mode control for cable-driven manipulators using time-delay estimation

Yaoyao Wang , Jiawei Peng , Kangwu Zhu , Bai Chen & Hongtao Wu

To cite this article: Yaoyao Wang , Jiawei Peng , Kangwu Zhu , Bai Chen & Hongtao Wu (2020): Adaptive PID-fractional-order nonsingular terminal sliding mode control for cable-driven manipulators using time-delay estimation, International Journal of Systems Science, DOI: 10.1080/00207721.2020.1808732

To link to this article: https://doi.org/10.1080/00207721.2020.1808732

Published online: 25 Aug 2020.

Submit your article to this journal

Article views: 20

View related articles

View Crossmark data

Full Terms & Conditions of access and use can be found at
https://www.tandfonline.com/action/journalInformation?journalCode=tsys20

INTERNATIONAL JOURNAL OF SYSTEMS SCIENCE
https://doi.org/10.1080/00207721.2020.1808732

Taylor & Francis
Taylor & Francis Group

Check for updates

Adaptive PID-fractional-order nonsingular terminal sliding mode control for cable-driven manipulators using time-delay estimation

Yaoyao Wang [a], Jiawei Peng [a], Kangwu Zhu [b], Bai Chen [a] and Hongtao Wu [a]

[a] National Key Laboratory of Science and Technology on Helicopter Transmission, Nanjing University of Aeronautics and Astronautics, Nanjing, People's Republic of China; [b] Shanghai Institute of Spaceflight Control Technology, Shanghai, People's Republic of China

ABSTRACT

This paper presents an adaptive proportional-integral-derivative fractional-order nonsingular terminal sliding mode (PID-FONTSM) control for the cable-driven manipulators using time-delay estimation (TDE). The proposed control uses TDE technique to obtain the lumped system dynamics and brings in an effective model-free structure. Then, a PID-FONTSM surface is designed to further enhance the control performance. The proposed PID-FONTSM surface uses the FONTSM error dynamic as its inner loop and utilises a PID-type surface with FONTSM variable as its outer loop. Benefitting from this structure, the proposed PID-FONTSM surface enjoys the advantages from both PID and FONTSM simultaneously. Afterwards, an adaptive algorithm is developed, to timely and precisely regulate the control gain for the robust term. The proposed control method is *model-free*, highly *accurate* and essentially *continuous* thanks to the TDE technique and developed PID-FONTSM surface and adaptive algorithm. The stability of the closed-loop control system under TDE and PID-FONTSM dynamics is proved using Lyapunov stability theory. Finally, comparative simulations were conducted to verify the effectiveness and superiorities of our proposed control method over the existing methods.

ARTICLE HISTORY
Received 14 September 2019
Accepted 5 August 2020

KEYWORDS
Adaptive control; PID; fractional-order nonsingular terminal sliding mode; FONTSM; PID-FONTSM; cable-driven manipulators

1. Introduction

Recently, cable-driven manipulators are becoming a research hotspot due to their obvious superiorities, such as large load-to-weight ratio and high flexibility and good safety for interactions with human beings (Shang et al., 2019; Townsend, 1988; Wang, Liu, Wang, et al., 2020; Wang, Yan, Chen, et al., 2019). Thanks to these advantages, cable-driven manipulators have huge potentials in medical treatment and personal nursing industry (Cui et al., 2017). Meanwhile, the control of cable-driven manipulators is still a challenging task because of the inevitable joint flexibility and complex system dynamics (Wang, Liu, Chen, et al., 2020; Wang, Yan, et al., 2020).

For accurate control of the systems with flexible joints, scholars have proposed some useful control methods (Babaghasabha et al., 2016; Huang & Chen, 2004; Korayem et al., 2017; Liu et al., 2018; Xu et al., 2018). In Xu et al. (2018), a dynamic control strategy was designed for a cable-driven hyper-redundant manipulator. The designed method utilises the pre-established detailed kinematics and dynamics and then ensures good control performance. For the precise control of cable-driven parallel robots with elastic cables, an adaptive robust control was designed (Babaghasabha et al., 2016). The adaptive robust control was based on the singular theory and requires the system dynamical model. An input–output feedback linearisation control method was proposed for a wheeled mobile cable-driven parallel robot, which has considered and utilised the dynamics from both parts (Korayem et al., 2017). To control a flexible joint robot without the detailed system dynamics, scholars developed a neuro-adaptive observer-based control (Liu et al., 2018). The proposed control applied Radial Basis Function (RBF) neural network to estimate the system dynamics, and then a dynamic surface control method was given. On the one hand, the above-mentioned control methods have guaranteed good comprehensive control for the systems with joint flexibilities. Small control errors and fast transient response have been obtained using these control

CONTACT Yaoyao Wang yywang_cmee@nuaa.edu.cn National Key Laboratory of Science and Technology on Helicopter Transmission, Nanjing University of Aeronautics and Astronautics, Yudao Road 29, Nanjing 210016, People's Republic of China

© 2020 Informa UK Limited, trading as Taylor & Francis Group

methods. On the other hand, system dynamics or complicated estimation algorithms are still required with the above-mentioned control methods. This requirement may bring about extra obstacles for practical applications.

To guarantee a simple but effective control of complex systems, scholars proposed the time-delay estimation (TDE) technique in the 1990s (Hsia, 1989; Hsia et al., 1991). By using the intentionally time-delayed information of the system to estimate the current lumped dynamics, the TDE can provide an effective model-free control structure. TDE can ensure satisfactory estimation accuracy. Due to these obvious superiorities, TDE has been utilised in lots of practical systems, such as robot manipulators (Baek et al., 2016, 2018; Jin et al., 2009; Jin, Kang, et al., 2017; Kali et al., 2018a, 2018b; Wang et al., 2016; Wang, Chen, et al., 2019; Wang, Li, et al., 2019, 2020; Wang, Yan, Zhu, et al., 2019; Wang, Zhu, et al., 2020), underwater vehicles (Kim et al., 2016), humanoid robots (Jin, Lee, et al., 2017; Roy et al., 2017) and exoskeleton (Han et al., 2018; Kim & Baek, 2017). In the meantime, the TDE technique will bring about large estimation errors when the systems have fast time-varying dynamics, such as Coulomb friction. Therefore, the TDE is usually utilised as a basic control structure to enjoy its model-free feature. Meanwhile, other robust control methods are used to reduce the potential estimation errors and guarantee high control performance under lumped uncertainties.

Several robust control structures can be effectively combined with TDE to pursue high control performance, such as sliding mode (SM) control (Jin et al., 2008; Roy & Kar, 2017), adaptive control (Alagoz et al., 2017; Baek et al., 2019; Han, 2020; Lochan et al., 2020; Tepljakov et al., 2018) and fuzzy logic method (Kim et al., 2017; Li & Yang, 2020; Li & Zhang, 2019). Meanwhile, the SM control has attracted much attention benefitting from its strong robustness against lumped uncertainties and simplicity for practical applications (Chen et al., 2013; Gao et al., 2020; Ibeas & Manuel, 2007; Utkin, 1993; Yu et al., 2005). To ensure strong robustness against unknown uncertainties, the SM control usually contains a discontinuous term with sufficiently large gain. This design will lead to a widely known issue, i.e. the *chattering* issue, which is still a main obstacle for practical implementation of SM control. To suppress the chattering issue and utilise SM control in practical applications, scholars have proposed several methods such as adaptive control (Ibeas & Manuel, 2006; Li & Chen, 2019; Yagmur & Alagoz, 2019), reaching law (Ma et al., 2019), backstepping technique (Tran et al., 2020) and intelligent methods (Fei & Lu, 2018; Lakhekar & Waghmare, 2018). In the meantime, the traditional SM control can only guarantee asymptotic convergence using a linear error dynamics. However, finite-time convergence has been widely verified to be more effective for lots of systems (Yu et al., 2005). Hence, some improved versions of SM control have been proposed and investigated, such as terminal SM (TSM) (Yu et al., 2005), nonsingular fast TSM (NFTSM) (Wang, Li, et al., 2020; Wang, Zhu, et al., 2020) and fractional-order NTSM (FONTSM) (Wang et al., 2016; Wang, Liu, Wang, et al., 2020; Wang, Yan, Chen, et al., 2019). By applying the aforesaid improved SM control structures, high control performance has been obtained. Recently, an adaptive fuzzy proportional-integral-derivative NFTSM (PID-NFTSM) control was proposed for uncertain nonlinear systems (Van, 2018). This method applies a hybrid PID-NFTSM surface to enhance the control and utilises an adaptive fuzzy logic element to estimate the system dynamics. Thanks to the two-loop structure of PID-NFTSM surface, the advantages of both NFTSM and PID methods can be enjoyed, such as highly accurate and fast transient response and singularity-free. On the other hand, the aforesaid adaptive fuzzy PID-NFTSM control still has two main problems: (1) the presented control is *singular* when $x_2 = 0$ or $\dot{e} = 0$ holds. This singularity issue comes from the proposed PID-NFTSM surface and will seriously damage the control performance; (2) the presented adaptive law is strictly non-decreasing, which means it will not decrease all the time. This may lead to overlarge control gain and obvious control performance degradation. What we need is a *simple*, *effective* and *singularity-free* control for cable-driven manipulators.

To further enhance the control performance of cable-driven manipulators under complex uncertainties, we propose an adaptive PID-FONTSM control using the TDE technique in this paper. The proposed control applies TDE as its basic structure and, therefore, ensures an effective model-free structure. Then, a PID-FONTSM surface is designed to guarantee high precision and fast transient response simultaneously. The proposed PID-FONTSM surface adopts a FONTSM error dynamic as its inner loop and utilises

a PID-type surface with FONTSM variable as its outer loop. Thanks to this structure, the proposed PID-FONTSM surface can enjoy the advantages from both PID and FONTSM. Afterwards, an adaptive algorithm is utilised to precisely regulate the control gain. The adaptive algorithm can timely reflect the current control performance and, therefore, satisfactory control performance can be ensured. The proposed control is *model-free* and highly *accurate* and essentially *continuous* thanks to the TDE technique and adaptive PID-FONTSM structure. The stability of the closed-loop control system under TDE and PID-FONTSM dynamics is analysed using the Lyapunov stability theory. Finally, comparative simulations were performed to demonstrate the superiorities of our control over the existing methods including the one from (Van, 2018).

The contributions of this work can be further emphasised

(1) to propose a PID-FONTSM surface, which successfully eliminates the singularity in the existing one from (Van, 2018);
(2) to propose an adaptive PID-FONTSM control using TDE, which is easy to use and can also assure high control performance;
(3) to prove the stability of the closed-loop control system considering TDE and PID-FONTSM dynamics;
(4) to verify the superiorities of our TDE-based adaptive PID-FONTSM control by comparative simulations.

The rest of this paper is structured as follows. Section 2 presents the problem description of this paper; meanwhile, Section 3 gives the proposed control design and some discussions. Then, comparative simulations are presented in Section 4. Finally, some conclusions are given in Section 5.

2. Problem description

The following equations are utilised to describe the cable-driven manipulators with n-DOF (degree of freedom) as (Wang, Liu, Wang, et al., 2020)

$$\mathbf{J}\ddot{\boldsymbol{\theta}} + \mathbf{D}_m\dot{\boldsymbol{\theta}} + \boldsymbol{\tau}_j = \boldsymbol{\tau} \tag{1}$$

$$\mathbf{M}(\mathbf{q})\ddot{\mathbf{q}} + \mathbf{C}(\mathbf{q},\dot{\mathbf{q}})\dot{\mathbf{q}} + \mathbf{G}(\mathbf{q}) + \mathbf{F}(\mathbf{q},\dot{\mathbf{q}}) + \boldsymbol{\tau}_d = \boldsymbol{\tau}_j \tag{2}$$

$$\mathbf{k}_p(\boldsymbol{\theta} - \mathbf{q}) + \mathbf{k}_d(\dot{\boldsymbol{\theta}} - \dot{\mathbf{q}}) = \boldsymbol{\tau}_j \tag{3}$$

Figure 1. The cable-driven manipulators being developed in our laboratory.

where $\mathbf{J} \in \mathrm{R}^{n\times n}$ and $\mathbf{D}_m \in \mathrm{R}^{n\times n}$ represent the inertia and damping matrices of drive motors, $\mathbf{q} \in \mathrm{R}^n$ and $\boldsymbol{\theta} \in \mathrm{R}^n$ are the position vectors of the joints and motors, respectively. $\boldsymbol{\tau}_j \in \mathrm{R}^n$ and $\boldsymbol{\tau} \in \mathrm{R}^n$ are the torque vectors generated by the joint compliance and drive motors, respectively. $\mathbf{M}(\mathbf{q}) \in \mathrm{R}^{n\times n}$ and $\mathbf{C}(\mathbf{q},\dot{\mathbf{q}}) \in \mathrm{R}^{n\times n}$ stand for the inertia and Coriolis/centrifugal matrices, $\mathbf{G}(\mathbf{q}) \in \mathrm{R}^n$ and $\mathbf{F}(\mathbf{q},\dot{\mathbf{q}}) \in \mathrm{R}^n$ represent the gravitational and friction vectors, respectively. $\boldsymbol{\tau}_d \in \mathrm{R}^n$ stands for the lumped uncertainties, including time-varying disturbance and unknown dynamics. Meanwhile, $\mathbf{k}_p \in \mathrm{R}^{n\times n}$ and $\mathbf{k}_d \in \mathrm{R}^{n\times n}$ are joint stiffness and damping matrices, respectively.

Substituting (2) into (1) and bringing in a constant $\bar{\mathbf{M}}$ yields

$$\bar{\mathbf{M}}\ddot{\mathbf{q}} + \mathbf{H} = \boldsymbol{\tau} \tag{4}$$

with $\mathbf{H}$ mathematically defined as

$$\begin{aligned}\mathbf{H} = {} & (\mathbf{M}(\mathbf{q}) - \bar{\mathbf{M}})\ddot{\mathbf{q}} + \mathbf{C}(\mathbf{q},\dot{\mathbf{q}})\dot{\mathbf{q}} + \mathbf{G}(\mathbf{q}) \\ & + \mathbf{F}(\mathbf{q},\dot{\mathbf{q}}) + \mathbf{J}\ddot{\boldsymbol{\theta}} + \mathbf{D}_m\dot{\boldsymbol{\theta}} + \boldsymbol{\tau}_d\end{aligned} \tag{5}$$

Note from (5) that $\mathbf{H}$ is used to describe all the system dynamics expect for $\bar{\mathbf{M}}\ddot{\mathbf{q}}$. $\mathbf{H}$ is quite complicated since it contains the rigid manipulator dynamics, the motor dynamics, the flexible dynamics and the unknown disturbance.

Then, the problem can be described as follows: to design a suitable control $\boldsymbol{\tau}$ for the cable-driven manipulators as shown in Figure 1 for example which can ensure accurate tracking of the reference trajectory $\mathbf{q}_d$ in a simple way.

Assumption 2.1: *The reference trajectory $\boldsymbol{q}_d$ is smooth, and thus its derivatives $\dot{\mathbf{q}}_d$ and $\ddot{\mathbf{q}}_d$ exist and bounded.*

Remark 2.1: The cable-driven manipulator considered in this work has a similar structure with the above twos, which are being optimised in our laboratory. As shown in Figure 1, the driven motors are installed in the base and the force is transmitted by cables. Thanks to this design, the moving inertial and energy consumption can be effectively reduced. Afterwards, good flexibility will also be guaranteed for cooperating with human being.

3. Proposed control method and discussions

To realise high performance control of cable-driven manipulators under lumped uncertainties, we propose an adaptive PID-FONTSM control based on TDE in this section. The proposed control uses TDE to estimate the system dynamics and then brings in an effective model-free structure. Then, a PID-FONTSM surface and an adaptive algorithm are developed to further enhance the control performance.

3.1. Proposed control method design

A PID-FONTSM surface is proposed in this section to utilise the advantages of PID and FONTSM dynamics. First, a FONTSM surface is selected as (Wang, Liu, Wang, et al., 2020)

$$\mathbf{s}_1 = \dot{\mathbf{e}} + \mathbf{a}_1 D^{\mathbf{b}_1}[\mathbf{sig}(\mathbf{e})^{\mathbf{c}_1}] + \mathbf{a}_2 D^{\mathbf{b}_2-1}[\mathbf{sig}(\mathbf{e})^{\mathbf{c}_2}] \quad (6)$$

where $\mathbf{e} = \mathbf{q}_d - \mathbf{q}$ stands for the error vector, $\mathbf{a}_1$ and $\mathbf{a}_2$ are constant diagonal matrices with positive elements; $\mathbf{b}_1, \mathbf{b}_2, \mathbf{c}_1$ and $\mathbf{c}_2$ are constant vectors and their elements are within (0,1). Meanwhile, the notations $\mathbf{sig}(\mathbf{x})^{\mathbf{y}}$ are defined as

$$\mathbf{sig}(\mathbf{x})^{\mathbf{y}} = [sig(x_1)^{y_1}, \ldots, sig(x_n)^{y_n}]^T \quad (7)$$

where $sig(x_i)^{y_i} = |x_i|^{y_i}\,\mathrm{sign}(x_i)$, $i = 1 \sim n$ and $\mathrm{sign}(x_i)$ stands for the sign function. It should be emphasised that $sig(x_i)^{y_i}$ is a continuous function with respect to x_i, and the corresponding proof can be found in (Yu et al., 2005).

Remark 3.1: By combining the fractional-order calculus with NTSM, the FONTSM surface (6) can assure faster convergence and higher accuracy than the widely used NTSM surface which has been experimentally verified (Wang et al., 2016; Wang, Liu, Wang, et al., 2020). Thus, we adopt the FONTSM surface as an inner surface to enjoy its high dynamical performance.

Afterwards, the proposed PID-FONTSM surface is given as

$$\mathbf{s}_2 = \mathbf{K}_p \mathbf{s}_1 + \mathbf{K}_i \int \mathbf{s}_1 + \mathbf{K}_d \dot{\mathbf{s}}_1 \quad (8)$$

where $\mathbf{K}_p$, $\mathbf{K}_i$ and $\mathbf{K}_d$ are constant diagonal matrices with positive elements.

Note from (6) that the designed surface is a combination of FONTSM and PID sliding variables. Thus, the advantages of both FONTSM and PID can be utilised. Meanwhile, the element $\dot{\mathbf{s}}_1$ can be given as

$$\dot{\mathbf{s}}_1 = \ddot{\mathbf{e}} + \mathbf{a}_1 D^{\mathbf{b}_1+1}[\mathbf{sig}(\mathbf{e})^{\mathbf{c}_1}] + \mathbf{a}_2 D^{\mathbf{b}_2}[\mathbf{sig}(\mathbf{e})^{\mathbf{c}_2}] \quad (9)$$

Substituting (9) into (8) and considering (4), we have

$$\begin{aligned}
\mathbf{s}_2 &= \mathbf{K}_p \mathbf{s}_1 + \mathbf{K}_i \int \mathbf{s}_1 + \mathbf{K}_d \dot{\mathbf{s}}_1 \\
&= \mathbf{K}_p \mathbf{s}_1 + \mathbf{K}_i \int \mathbf{s}_1 + \mathbf{K}_d \ddot{\mathbf{e}} \\
&\quad + \mathbf{K}_d(\mathbf{a}_1 D^{\mathbf{b}_1+1}[\mathbf{sig}(\mathbf{e})^{\mathbf{c}_1}] + \mathbf{a}_2 D^{\mathbf{b}_2}[\mathbf{sig}(\mathbf{e})^{\mathbf{c}_2}]) \\
&= \mathbf{K}_p \mathbf{s}_1 + \mathbf{K}_i \int \mathbf{s}_1 + \mathbf{K}_d(\ddot{\mathbf{q}}_d - \bar{\mathbf{M}}^{-1}(\boldsymbol{\tau} - \mathbf{H})) \\
&\quad + \mathbf{K}_d(\mathbf{a}_1 D^{\mathbf{b}_1+1}[\mathbf{sig}(\mathbf{e})^{\mathbf{c}_1}] + \mathbf{a}_2 D^{\mathbf{b}_2}[\mathbf{sig}(\mathbf{e})^{\mathbf{c}_2}])
\end{aligned} \quad (10)$$

To ensure fast convergence of the PID-FONTSM variable, we design the following adaptive reaching law as

$$\dot{\mathbf{s}}_2 = -(\hat{\mathbf{k}}_1 + \bar{\mathbf{k}}_1)\mathbf{sign}(\mathbf{s}_2) \quad (11)$$

where $\bar{\mathbf{k}}_1$ is a diagonal constant matrix with positive elements, and $\hat{\mathbf{k}}_1$ is a diagonal matrix with adaptive positive elements as

$$\dot{\hat{k}}_{1i} = \begin{cases} -\eta_i |s_{2i}|, \text{ if } \hat{k}_{1i} = k_{1i\max} \\ \beta(s_{2i}), \text{ if } k_{1i\min} < \hat{k}_{1i} < k_{1i\max} \\ \eta_i |s_{2i}|, \text{ if } \hat{k}_{1i} = k_{1i\min} \end{cases} \quad (12)$$

where $\beta(s_{2i}) = \eta_i |s_{2i}|$ under $|s_{2i}| \geq \Phi_i$ and $\beta(s_{2i}) = -(\eta_i |s_{2i}| + \Delta_i)^{-1}$ under $|s_{2i}| < \Phi_i$, $\Phi_i > 0$, $0 < k_{1imin} < k_{1imax}$ are the maximum and minimum value of the adaptive gain $\hat{k}_{1i}$. The $\Delta_i > 0$ is a small constant used to avoid infinite adaptive rate when $s_{2i} = 0$ holds.

Note from (11) that the adaptive reaching law contains both constant and adaptive gains, i.e. $\bar{\mathbf{k}}_1$ and $\hat{\mathbf{k}}_1$.

The former is used to guarantee basic performance, while the latter is applied to obtain good robustness against time-varying uncertainties. It can be observed from (12) that the adaptive algorithm can timely and precisely regulate the gain $\hat{k}_{1i}$. To be specific, $\hat{k}_{1i}$ will increase when the control performance is not satisfactory, *i.e.* $|s_{2i}| > \Phi_i$; otherwise, it will rapidly decrease to ensure smooth control. Meanwhile, the adaptive gain $\hat{k}_{1i}$ is manually restricted within a pre-designed field $[k_{1imin}, k_{1imax}]$. This design is mainly used to suppress the potential control performance degradation.

If no restrictions are made, the adaptive gain $\hat{k}_{1i}$ may increase/decrease to an inappropriately large/small one after long-time running, and the control performance may degrade.

Then, the adaptive PID-FONTSM control is designed as

$$\begin{aligned}\boldsymbol{\tau} &= \bar{\mathbf{M}}\mathbf{u} + \hat{\mathbf{H}}\\ \mathbf{u} &= \ddot{\mathbf{q}}_d + \mathbf{a}_1 D^{\mathbf{b}_1+1}[\mathbf{sig}(\mathbf{e})^{\mathbf{c}_1}] + \mathbf{a}_2 D^{\mathbf{b}_2}[\mathbf{sig}(\mathbf{e})^{\mathbf{c}_2}]\\ &\quad + \mathbf{K}_d{}^{-1}\left(\mathbf{K}_p\mathbf{s}_1 + \mathbf{K}_i\int \mathbf{s}_1 + \int (\hat{\mathbf{k}}_1 + \bar{\mathbf{k}}_1)\mathbf{sign}(\mathbf{s}_2)\right)\end{aligned} \tag{13}$$

where $\hat{\mathbf{H}}$ represents the estimation of $\mathbf{H}$ described in (5).

Therefore, the control objective will be accomplished if we can obtain $\hat{\mathbf{H}}$ precisely and timely. However, $\mathbf{H}$ is highly complex, as shown in (5), and can be very difficult to obtain using traditional methods. To effectively settle this issue, we apply TDE to estimate $\mathbf{H}$ in a simple structure as

$$\hat{\mathbf{H}}(t) \cong \mathbf{H}(t-L) \tag{14}$$

where L stands for the delayed time and is usually set as one or several sampling periods. By using the intentionally time-delayed information of the system, $\mathbf{H}$ can be properly estimated in a straightforward way.

Substituting (4) into (14), we have

$$\hat{\mathbf{H}}(t) \cong \boldsymbol{\tau}(t-L) - \bar{\mathbf{M}}\ddot{\mathbf{q}}(t-L) \tag{15}$$

As shown in (15), two variables $\boldsymbol{\tau}(t-L)$ and $\ddot{\mathbf{q}}(t-L)$ are required to perform TDE. The former can be easily acquired using the control signal $\boldsymbol{\tau}$, while the latter can be obtained using numerical differentiation (Wang, Liu, Wang, et al., 2020). To suppress the enlarged noise effect from the above numerical differentiation, smaller control gain $\bar{\mathbf{M}}$ or low-pass filter can be used (Baek et al., 2016; Jin et al., 2009; Wang et al., 2016). Moreover, no system dynamics are required in (15) to obtain $\mathbf{H}$, thus the TDE can assure an effective model-free structure.

Combining (13) and (15), the TDE-based adaptive PID- FONTSM control is proposed as

$$\boldsymbol{\tau} = \bar{\mathbf{M}}\mathbf{u} + \boldsymbol{\tau}(t-L) - \bar{\mathbf{M}}\ddot{\mathbf{q}}(t-L) \tag{16}$$

with $\mathbf{u}$ given in (13). Then, the block diagram of our proposed PID-FONTSM control is given in Figure 2.

Note from (13) and (16) that no system dynamics are utilised in the proposed control. Therefore, it is not a model-based control strategy and should be regarded as a model-free one instead. Meanwhile, the developed control is also essentially continuous since the sign function is behind the integral operator. Furthermore, the proposed control can ensure high control performance thanks to the proposed PID-FONTSM surface and adaptive algorithm. To conclude, the proposed control is *model-free*, *accurate* and *continuous*.

Remark 3.2: Analysing the system dynamics (4) and TDE (14)–(15), we can observe that the system contains no time-delayed dynamics and the time delay L is intentionally introduced into the control system. It should be emphasised that the TDE (14)–(15) is not used to estimate the delayed time L, and it is applied to estimate the lumped system dynamics by utilising time-delayed signals. Thanks to TDE, a practical model-free control structure is established. Usually, the delayed time L is selected sufficiently small and then the stability of the closed-loop control system will not be affected. The corresponding theoretical analysis of the effect by TDE, i.e. TDE error, is given in the appendix.

Remark 3.3: Comparing (5) with (14) and (15), we can see that the variables $\dot{\boldsymbol{\theta}}$ and $\ddot{\boldsymbol{\theta}}$ shown in (5) disappear in the TDE structure (14)–(15). Note from (5) that $\ddot{\mathbf{q}}$ and $\ddot{\boldsymbol{\theta}}$ and $\mathbf{H}$ are coupled. Thus, the effect of $\dot{\boldsymbol{\theta}}$ and $\ddot{\boldsymbol{\theta}}$ is still considered in (14)–(15) through the acceleration signal $\ddot{\mathbf{q}}$.

3.2. Comparisons with the existing adaptive PID-NFTSM control method

The proposed control (16) is inspired by the one given in (Van, 2018), which will be briefly given in what follows.

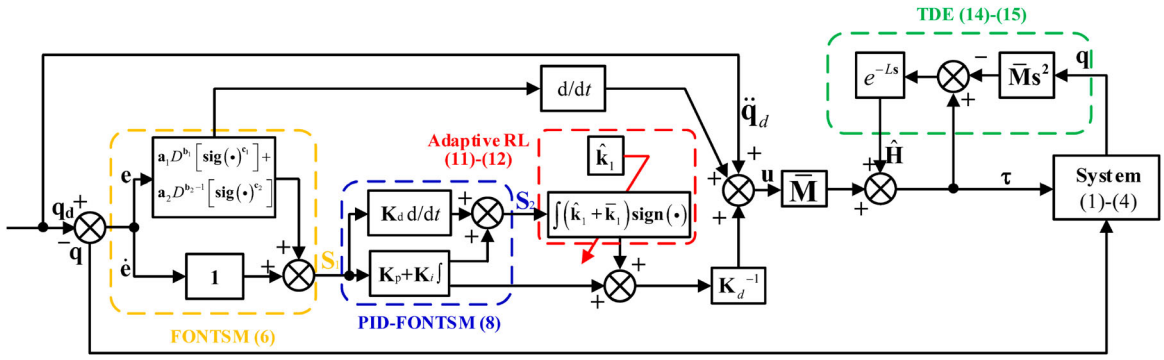

Figure 2. Block diagram of our proposed PID-FONTSM control (13).

First, the NFTSM surface was selected as

$$\mathbf{s}_3 = \mathbf{e} + \bar{\mathbf{a}}_1 \mathbf{sig}(\mathbf{e})^{\bar{\mathbf{c}}_1} + \bar{\mathbf{a}}_2 \mathbf{sig}(\dot{\mathbf{e}})^{\bar{\mathbf{c}}_2} \tag{17}$$

where $\bar{\mathbf{a}}_1$ and $\bar{\mathbf{a}}_2$ are diagonal matrices with positive elements, $\bar{\mathbf{c}}_1$ and $\bar{\mathbf{c}}_2$ are constant vectors with elements satisfying $\bar{c}_{1i} > \bar{c}_{2i}, 1 < \bar{c}_{2i} < 2$. Note that $\mathbf{s}_3$ (17) is continuous with respect to $\mathbf{e}$ and $\dot{\mathbf{e}}$ considering the definition of the function $\mathrm{sig}(x)^y$.

Then, the PID-NFTSM surface was designed as (Van, 2018)

$$\mathbf{s}_4 = \bar{\mathbf{K}}_p \mathbf{s}_3 + \bar{\mathbf{K}}_i \int \mathbf{s}_3 + \bar{\mathbf{K}}_d \dot{\mathbf{s}}_3 \tag{18}$$

where $\bar{\mathbf{K}}_p$, $\bar{\mathbf{K}}_i$ and $\bar{\mathbf{K}}_d$ are constant diagonal matrices with positive elements.

Combining (4), (17) and (18), we have

$$\begin{aligned}\mathbf{s}_4 &= \bar{\mathbf{K}}_p \mathbf{s}_3 + \bar{\mathbf{K}}_i \int \mathbf{s}_3 \\ &\quad + \bar{\mathbf{K}}_d(\dot{\mathbf{e}} + \bar{\mathbf{a}}_1\bar{\mathbf{c}}_1|\mathbf{e}|^{\bar{\mathbf{c}}_1-1}\dot{\mathbf{e}} + \bar{\mathbf{a}}_2\bar{\mathbf{c}}_2|\dot{\mathbf{e}}|^{\bar{\mathbf{c}}_2-1}(\ddot{\mathbf{q}}_d - \ddot{\mathbf{q}})) \\ &= \bar{\mathbf{K}}_p \mathbf{s}_3 + \bar{\mathbf{K}}_i \int \mathbf{s}_3 \\ &\quad + \bar{\mathbf{K}}_d(\dot{\mathbf{e}} + \bar{\mathbf{a}}_1\bar{\mathbf{c}}_1|\mathbf{e}|^{\bar{\mathbf{c}}_1-1}\dot{\mathbf{e}} + \bar{\mathbf{a}}_2\bar{\mathbf{c}}_2|\dot{\mathbf{e}}|^{\bar{\mathbf{c}}_2-1} \\ &\quad \times (\ddot{\mathbf{q}}_d - \bar{\mathbf{M}}^{-1}(\boldsymbol{\tau} - \mathbf{H}))) \end{aligned} \tag{19}$$

For reaching law, the following adaptive one was applied

$$\dot{\mathbf{s}}_4 = -(\hat{\mathbf{k}}_2 + \bar{\mathbf{k}}_2)\mathbf{sign}(\mathbf{s}_4) \tag{20}$$

where $\bar{\mathbf{k}}_2$ is a diagonal constant matrix with positive elements, and $\hat{\mathbf{k}}_2$ is a diagonal matrix with adaptive positive elements as

$$\dot{\hat{k}}_{2i} = \bar{\eta}_i |s_{4i}| \tag{21}$$

where $\bar{\eta}_i$ is a positive constant.

Eventually, the adaptive PID-NFTSM control was designed as (Van, 2018)

$$\begin{aligned}\boldsymbol{\tau} &= \bar{\mathbf{M}}\mathbf{u} + \hat{\mathbf{H}} \\ \mathbf{u} &= \ddot{\mathbf{q}}_d + \bar{\mathbf{a}}_2^{-1}\bar{\mathbf{c}}_2^{-1}|\dot{\mathbf{e}}|^{2-\bar{\mathbf{c}}_2}(1 + \bar{\mathbf{a}}_1\bar{\mathbf{c}}_1|\mathbf{e}|^{\bar{\mathbf{c}}_1-1}) \\ &\quad + \bar{\mathbf{a}}_2^{-1}\bar{\mathbf{c}}_2^{-1}\bar{\mathbf{K}}_d^{-1}|\dot{\mathbf{e}}|^{1-\bar{\mathbf{c}}_2} \\ &\quad \times \left(\bar{\mathbf{K}}_p\mathbf{s}_3 + \bar{\mathbf{K}}_i \int \mathbf{s}_3 + (\hat{\mathbf{k}}_2 + \bar{\mathbf{k}}_2) \int \mathbf{sign}(\mathbf{s}_4)\right)\end{aligned} \tag{22}$$

where $\hat{\mathbf{H}}$ represents the estimation of $\mathbf{H}$. To make the comparisons fair and convincing, we also apply the TDE technique here to obtain $\mathbf{H}$.

Then, the comparisons between our proposed method and the existing one will be conducted in the following two aspects.

(1) *Sliding surface*: Our proposed method uses a FONTSM surface as its inner sliding variable, while the existing method utilises a traditional NFTSM surface. It has been widely proved that the FONTSM surface can guarantee a better comprehensive performance than the traditional NFTSM surface (Wang et al., 2016; Wang, Liu, Wang, et al., 2020). On the other hand, *singularity* issue has been generated with the NFTSM surface. As shown in (22), the control effort $\mathbf{u}$ contains an element $|\dot{\mathbf{e}}|^{1-\bar{\mathbf{c}}_2}$ which will bring in a serious singularity problem at $\dot{\mathbf{e}} = 0$ considering $1 < \bar{c}_{2i} < 2$. This singularity issue can seriously damage the control performance and even the system hardware. For comparisons, our proposed control is totally *singularity-free* thanks to the FONTSM surface.

(2) *Adaptive algorithm*: Our proposed control and the existing one both utilise adaptive algorithms to

regulate the control gain. However, the adaptive algorithm (21) from Van (2018) is strictly non-decreasing and may lead to overlarge adaptive gain $\hat{k}_{2i}$. This may seriously degrade the control performance after long-time running. For comparison, our adaptive algorithm (12) can timely and precisely regulate the adaptive gain $\hat{k}_{1i}$ based on current control performance.

Thus, our proposed TDE-based adaptive PID-FONTSM control can ensure better comprehensive control performance than the existing adaptive PID-NFTSM control thanks to the PID-FONTSM surface and adaptive algorithm. The above claims will be verified by comparative simulations in the next section.

Remark 3.4: Taking the element $|\dot{\mathbf{e}}|^{1-\bar{\mathbf{c}}_2}$ to analyse, we can see that $|\dot{\mathbf{e}}|^{1-\bar{\mathbf{c}}_2} = +\infty$ will hold under $\dot{\mathbf{e}} = 0$ and $1 < \bar{c}_{2i} < 2$. For example, when $\bar{c}_{2i} = 1.5$, we have $|\dot{\mathbf{e}}|^{1-\bar{\mathbf{c}}_2} \approx 10^4$ under $|\dot{\mathbf{e}}| = 10^{-8}$ and $|\dot{\mathbf{e}}|^{1-\bar{\mathbf{c}}_2} \approx 10^3$ under $|\dot{\mathbf{e}}| = 10^{-6}$. Therefore, when the system trajectory fluctuates around $|\dot{\mathbf{e}}| = 0$, the element $|\dot{\mathbf{e}}|^{1-\bar{\mathbf{c}}_2}$ and corresponding control effort $\mathbf{u}$ will fluctuate sharply which will result in the singularity issue for the system.

3.3. Stability analysis

In this subsection, the stability of the closed-loop control system under TDE and PID-FONTSM dynamics is analysed using Lyapunov stability theory. Substituting the proposed control (13) into the PID-FONTSM surface (8), we have

$$\begin{aligned}\mathbf{s}_2 &= \mathbf{K}_p\mathbf{s}_1 + \mathbf{K}_i\int \mathbf{s}_1 + \mathbf{K}_d(\ddot{\mathbf{q}}_d - \bar{\mathbf{M}}^{-1}(\boldsymbol{\tau} - \mathbf{H})) \\ &\quad + \mathbf{K}_d(\mathbf{a}_1 D^{\mathbf{b}_1+1}[\mathbf{sig}(\mathbf{e})^{\mathbf{c}_1}] + \mathbf{a}_2 D^{\mathbf{b}_2}[\mathbf{sig}(\mathbf{e})^{\mathbf{c}_2}]) \\ &= -\mathbf{K}_d\bar{\mathbf{M}}^{-1}(\hat{\mathbf{H}} - \mathbf{H}) - \int (\hat{\mathbf{k}}_1 + \bar{\mathbf{k}}_1)\mathbf{sign}(\mathbf{s}_2) \\ &= \mathbf{K}_d\boldsymbol{\varepsilon} - \int (\hat{\mathbf{k}}_1 + \bar{\mathbf{k}}_1)\mathbf{sign}(\mathbf{s}_2) \end{aligned} \tag{23}$$

where $\boldsymbol{\varepsilon} = -\bar{\mathbf{M}}^{-1}(\hat{\mathbf{H}} - \mathbf{H})$ stands for the bounded estimation error caused by TDE, and its first-order derivative $\dot{\boldsymbol{\varepsilon}}$ is also bounded as $|\dot{\varepsilon}_i| \le \Omega_i$. The boundedness proof of $\boldsymbol{\varepsilon}$ and $\dot{\boldsymbol{\varepsilon}}$ can be found in (Jin et al., 2009; Kali et al., 2018b). For the integrity of this paper, we give brief bounded proof of $\boldsymbol{\varepsilon}$ and $\dot{\boldsymbol{\varepsilon}}$ in the appendix. For simplicity, we will take the ith-DOF (degree of freedom) to analyse.

Select the following Lyapunov function as

$$V_i = \frac{1}{2}s_{2i}^2 + \frac{1}{2}\tilde{k}_{1i}^2 \tag{24}$$

where $\tilde{k}_{1i} = k_{1i\max} - \hat{k}_{1i} \ge 0$. Note that $\tilde{k}_{1i}$ stands for estimation error between the pre-design maximum value k_{1imax} and our proposed adaptive gain $\hat{k}_{1i}$.

Differentiating (24) along time and considering (23) yields

$$\begin{aligned}\dot{V}_i &= s_{2i}\dot{s}_{2i} - \tilde{k}_{1i}\dot{\hat{k}}_{1i} \\ &= s_{2i}(K_{di}\dot{\varepsilon}_i - (\hat{k}_{1i} + \bar{k}_{1i})\mathrm{sign}(s_{2i})) - \tilde{k}_{1i}\dot{\hat{k}}_{1i} \\ &= -(\hat{k}_{1i} + \bar{k}_{1i})|s_{2i}| + K_{di}\dot{\varepsilon}_i s_{2i} - \tilde{k}_{1i}\dot{\hat{k}}_{1i} \end{aligned} \tag{25}$$

Since $|\dot{\varepsilon}_i| \le \Omega_i$, properly select $\bar{k}_{1i}$ such that $\bar{k}_{1i} \ge K_{di}\Omega_i$. Then, (25) becomes

$$\dot{V}_i \le -\hat{k}_{1i}|s_{2i}| - \tilde{k}_{1i}\dot{\hat{k}}_{1i} \tag{26}$$

Considering $\tilde{k}_{1i} \ge 0$, therefore, the stability condition (26) will be further enhanced when $\dot{\hat{k}}_{1i} \ge 0$ holds. Therefore, we will take the condition $\dot{\hat{k}}_{1i} < 0$ to analyse which has two cases.

Case one: $\dot{\hat{k}}_{1i} = -\eta_i|s_{2i}|$, i.e. $\hat{k}_{1i}$=$k_{1i\max}$, holds. Under this case, we have $\tilde{k}_{1i} = 0$. Then, (26) becomes $\dot{V}_i \le -\hat{k}_{1i}|s_{2i}|$. Therefore, the system trajectory will continue converging to the equilibrium point until $s_{2i} = 0$.

Case two: $\dot{\hat{k}}_{1i} = -(\eta_i|s_{2i}| + \Delta_i)^{-1}$ holds, *i.e.* $k_{1i\min} < \hat{k}_{1i} < k_{1imax}$ and $|s_{2i}| < \Phi_i$. Then, (26) can be rewritten as

$$\dot{V}_i \le -\frac{\hat{k}_{1i}|s_{2i}|(\eta_i|s_{2i}| + \Delta_i) - \tilde{k}_{1i}}{(\eta_i|s_{2i}| + \Delta_i)} \le -\frac{\hat{k}_{1i}\Delta_i|s_{2i}| - \tilde{k}_{1i}}{(\eta_i|s_{2i}| + \Delta_i)} \tag{27}$$

We can observe from (27) that $\dot{V}_i < 0$ will always hold under $|s_{2i}| > \tilde{k}_{1i}\hat{k}_{1i}^{-1}\Delta_i{}^{-1}$. Therefore, the system trajectory s_{2i} will persistently converge to the following field until the condition $\dot{V}_i < 0$ is unsatisfied under case two as

$$|s_{2i}| \le \min(\tilde{k}_{1i}\hat{k}_{1i}^{-1}\Delta_i{}^{-1}, \Phi_i) \tag{28}$$

Combining the results from the above two cases, we can see that the PID-FONTSM variable s_{2i} will be bounded using our proposed control (13). Then, the FONTSM surface s_{1i} will also be bounded with the proper selection of K_{pi}, K_{ii} and K_{di}. Afterwards, according to the theoretical results from (Wang et al.,

2018) concerning the FONTSM surface, the tracking error e_i and $\dot{e}_i$ will also be bounded. Finally, the stability under TDE and PID-FONTSM dynamics is proved.

4. Simulation verifications

4.1. Verification set-up

To test the effectiveness and advantages of our proposed control method, comparative simulations have been performed.

For the dynamics of cable-driven manipulators, the rigid part described by (2) is directly taken from (Jin et al., 2009) as

$$\begin{aligned}\mathbf{M}(\mathbf{q})_{11} &= l_2^2 m_2 + 2l_1 l_2 m_2 c_2 + l_1^2(m_1+m_2),\\ &\times \mathbf{M}(\mathbf{q})_{22} = l_2^2 m_2\\ \mathbf{M}(\mathbf{q})_{12} &= \mathbf{M}(\mathbf{q})_{21} = l_2^2 m_2 + l_1 l_2 m_2 c_2\end{aligned} \tag{29}$$

$$\mathbf{C}(\mathbf{q},\dot{\mathbf{q}})\dot{\mathbf{q}} = \begin{bmatrix} -l_1 l_2 m_2 s_2 \dot{q}_2^2 - 2l_1 l_2 m_2 s_2 \dot{q}_1 \dot{q}_2 \\ l_1 l_2 m_2 s_2 \dot{q}_2^2 \end{bmatrix} \tag{30}$$

$$\mathbf{G}(\mathbf{q}) = \begin{bmatrix} l_2 m_2 g c_{12} + l_1(m_1+m_2) g c_1 \\ l_2 m_2 g c_{12} \end{bmatrix} \tag{31}$$

$$\mathbf{F}(\mathbf{q},\dot{\mathbf{q}}) = \begin{bmatrix} F_{v1}\dot{q}_1 + F_{c1} sign(\dot{q}_1) \\ F_{v2}\dot{q}_2 + F_{c2} sign(\dot{q}_2) \end{bmatrix} \tag{32}$$

where l_i, m_i, F_{vi} and F_{ci} represent the link length, mass, viscous and Coulomb friction coefficients for the ith-DOF, respectively; g stands for the local acceleration, and $s_i = \sin(q_i)$, $c_i = \cos(q_i)$, and $c_{ij} = \cos(q_i + q_j)$. Specifically, $m_1 = m_2 = 1\,\text{kg}$, $l_1 = 1\,\text{m}$, $l_2 = 0.8\,\text{m}$, $F_{v1} = F_{v2} = 5\,\text{N·m·s/rad}$, $F_{c1} = F_{c2} = 5\,\text{N·m}$, $g = 9.8\,\text{m/s}^2$ are used in the following simulations. The flexible parts by (1) and (3) are given as $\mathbf{J} = [0.5, 0; 0, 0.2]\,\text{kg·m}^2$, $\mathbf{D}_\text{m} = [0.1, 0; 0, 0.02]\,\text{N·m·s/rad}$, $\mathbf{k}_p = [2, 0; 0, 1]\ 10^4\,\text{N·m/rad}$, $\mathbf{k}_d = [50, 0; 0, 40]\,\text{N·m·s/rad}$. Moreover, a disturbance signal $\boldsymbol{\tau}_d = \sin(\pi t/2)\,\text{N·m}$ is added to both joints to verify the robustness of the control methods.

For comparisons, five controllers have been simulated which are our proposed control (16), Van's control (22), two PID controllers with different gains and a TDE-based SM control. For fairness, TDE is also utilised for Van's control. Moreover, the traditional TDE-based SM control is given as

$$\boldsymbol{\tau} = \bar{\mathbf{M}}[\ddot{\mathbf{q}}_d + \boldsymbol{\lambda}_1\dot{\mathbf{e}} + \mathbf{K}\mathbf{sign}(\mathbf{s})] + \boldsymbol{\tau}(t-L) - \bar{\mathbf{M}}\ddot{\mathbf{q}}(t-L) \tag{33}$$

with SM surface defined as $\mathbf{s} = \dot{\mathbf{e}} + \boldsymbol{\lambda}_1\mathbf{e}$. To suppress chatters caused by the sign function, we utilised the saturation function with a boundary $\boldsymbol{\varphi}$. Two simulations were conducted. In simulation one, a combined sinusoidal signal is given as reference trajectory. In simulation two, the manipulator is commanded to track a triangular wave signal. It should be noted that the disturbance $\boldsymbol{\tau}_d$ is considered in both simulations.

The parameters for the above controllers are given in Table 1. Note $\mathbf{a}_1 = \mathbf{a}_2 = \bar{\mathbf{a}}_1 = \bar{\mathbf{a}}_2$, $\bar{\mathbf{c}}_1 = \bar{\mathbf{c}}_2 = \mathbf{c}_1{}^{-1} = \mathbf{c}_2{}^{-1}$, $\lambda_1 = \mathbf{a}_1 + \mathbf{a}_2$ are satisfied to assure the comparison fairness. Define

$$\begin{aligned}\bar{\mathbf{u}} &= \bar{\mathbf{a}}_2^{-1}\bar{\mathbf{c}}_2^{-1}\bar{\mathbf{K}}_d^{-1}|\dot{\mathbf{e}}|^{1-\bar{\mathbf{c}}_2}\\ &\times\left(\bar{\mathbf{K}}_p\mathbf{s}_3 + \bar{\mathbf{K}}_i\int \mathbf{s}_3 + (\hat{\mathbf{k}}_2 + \bar{\mathbf{k}}_2)\int \mathbf{sign}(\mathbf{s}_4)\right)\end{aligned} \tag{34}$$

for simplicity and it will be used in the following figures.

4.2. Results and discussions

(1) *Simulation one:* the desired trajectory $\mathbf{q}_d$ is given as $\mathbf{q}_d = \sin(\pi t/6) + \sin(\pi t/8)$ for both joints. Then, we can observe that the $\mathbf{q}_d(t=0) = \mathbf{0}$, $\dot{\mathbf{q}}_d(t=0) = \text{diag}(7\pi,\ 7\pi)/24\,\text{rad/s}$. Since Van's control (22) has singularity issue, the initial value of $\dot{\mathbf{e}}$ must be non-zero to ensure the successful execution of the simulations. Finally, the control results are given in Figures 3–9.

As shown in Figures 3 and 5, a good control performance has been obtained with all five controllers.

Table 1. Parameters of comparative five controllers.

Controller	Parameters
Our Control (16)	$\mathbf{a}_1 = \mathbf{a}_2 = \text{diag}(1,1)$, $\mathbf{b}_1 = 0.01\times\text{diag}(1,1)$, $\mathbf{b}_2 = \text{diag}\ (0.99,0.99)$, $\mathbf{c}_1 = \mathbf{c}_2 = \text{diag}(0.8,0.8)$, $\mathbf{K}_p = \text{diag}(60, 60)$, $\mathbf{K}_i = \text{diag}(0.4,0.5)$, $\mathbf{K}_d = \text{diag}\ (4,2)$, $\bar{\mathbf{k}}_1 = \text{diag}\ (2,2)$, $\boldsymbol{\eta} = \text{diag}(1,1)$, $\boldsymbol{\Phi} = 0.1\times\text{diag}(1, 1)$, $\Delta = 0.01\times\text{diag}(4, 4)$, $\mathbf{k}_{1min} = \text{diag}\ (1, 1)$, $\mathbf{k}_{1max} = \text{diag}\ (10,10)$, $\bar{\mathbf{M}} = \text{diag}(0.15, 0.15)$, $\hat{\mathbf{k}}_1(t=0) = \mathbf{k}_{1min}$, $\boldsymbol{\theta}(t=0) = \dot{\boldsymbol{\theta}}(t=0) = \mathbf{0}$, $\mathbf{q}(t=0) = [-5, -5]$ deg, $\dot{\mathbf{q}}(t=0) = [60, 60]$degree/s, $L = 1$ ms.
Van's Control (22)	$\bar{\mathbf{a}}_1 = \bar{\mathbf{a}}_2 = \text{diag}(1,1)$, $\bar{\mathbf{c}}_1 = \bar{\mathbf{c}}_2 = \text{diag}\ (1.25,1.25)$, $\bar{\boldsymbol{\eta}} = \text{diag}(0.6,0.6)$ and others remain the same as the ones of our control.
PID 1	$\mathbf{K}_p = \mathbf{K}_i = 10^3\times\text{diag}(1.5, 1.5)$, $\mathbf{K}_d = \text{diag}(50, 50)$
PID 2	$\mathbf{K}_p = \mathbf{K}_i = 10^3\times\text{diag}\ (2, 2)$, $\mathbf{K}_d = \text{diag}(20, 20)$
TDE-based SM Control	$\lambda_1 = \text{diag}(2,2)$, $\mathbf{K} = \text{diag}(1,1)$, $\boldsymbol{\varphi} = \text{diag}(0.1, 0.05)$ and others remain the same as ours

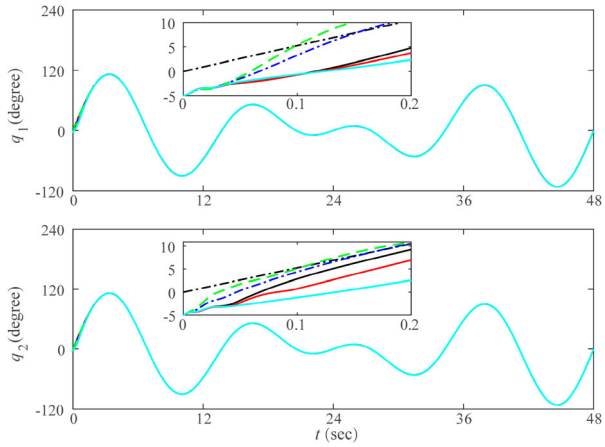

Figure 3. Trajectory tracking performance under sinusoidal signal: reference trajectory (black dashdot), our proposed control (black solid), Van's control (red solid), PID 1 (blue dashdot), PID 2 (green dashed) and TDE-based SMC scheme (cyan solid).

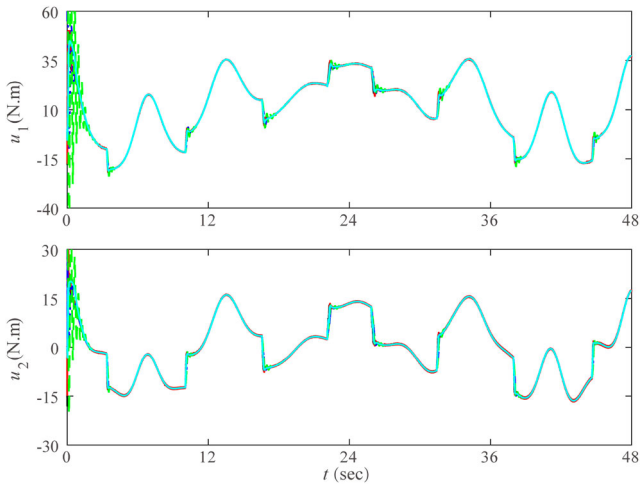

Figure 5. Control efforts under sinusoidal signal: our proposed control (black solid), Van's control (red solid), PID 1 (blue dashdot), PID 2 (green dashed) and TDE-based SMC scheme (cyan solid).

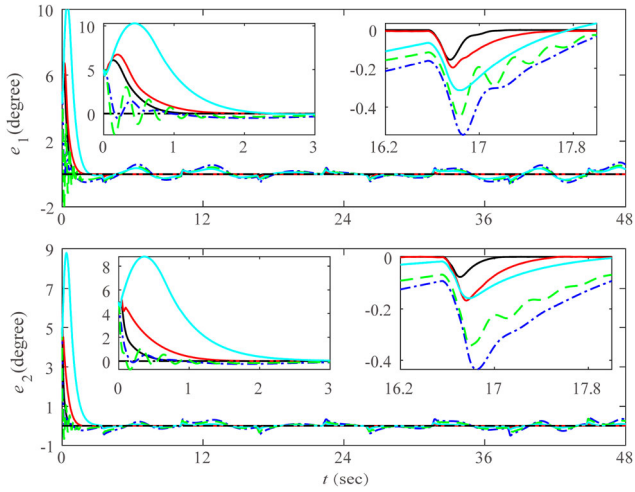

Figure 4. Tracking error under sinusoidal signal: our proposed control (black solid), Van's control (red solid), PID 1 (blue dashdot), PID 2 (green dashed) and TDE-based SMC scheme (cyan solid).

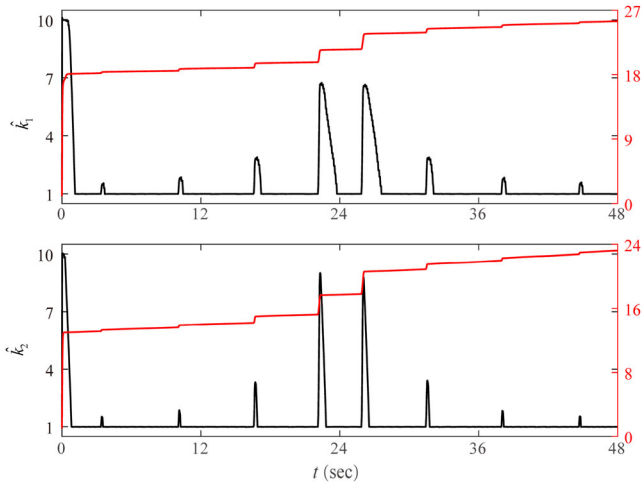

Figure 6. Adaptive gain $\hat{\mathbf{k}}$ under sinusoidal signal: our proposed control (black solid) and Van's control (red solid).

High precision and fast convergence have been clearly observed. This strongly demonstrates the effectiveness of TDE, SM, PID, existing PID-NFTSM and our proposed PID-FONTSM surfaces. In the meantime, our PID-FONTSM surface and its corresponding control can assure the best comprehensive control performance among all five controllers, as shown in Figures 4 and 5. To clearly show the performance, we will analyse Figures 4 and 5 afterwards. In the initial phase, two PID controllers with large gains can provide the fastest convergence, as shown in Figure 4. However, obvious large fluctuations in the initial phase have also been observed due to the large control gains, as shown in Figures 4 and 5. For comparison, our proposed control can ensure smooth fast convergence in the initial phase. In the steady phase, our control assures the highest tracking precision, while the PID controllers provide relative the worst, as shown in Figure 4. Thus, our proposed control assures the best comprehensive control performance among all five controllers.

Taking Figures 6 and 7 to analyse, we can see that large TDE error will occur when the desired trajectory tends to turn around. This is mainly caused by the frictions and will lead to large control errors, as shown in Figure 4. Therefore, adaptive algorithms are used to suppress the TDE errors, as indicated in Figure 6.

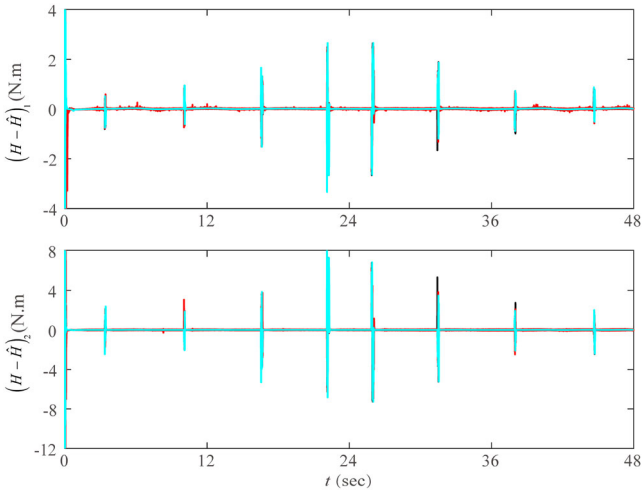

Figure 7. TDE error element ($\mathbf{H} - \hat{\mathbf{H}}$) under sinusoidal signal: our proposed control (black solid), Van's control (red solid) and TDE-based SMC scheme (cyan solid).

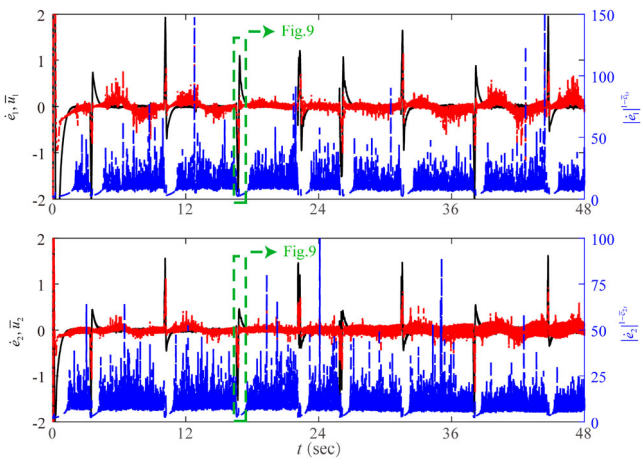

Figure 8. Speed tracking error $\dot{\mathbf{e}}$(left y-axis, black solid), control element $\bar{\mathbf{u}}$ (red dashdot, left y-axis) and $|\dot{\mathbf{e}}|^{1-\bar{\mathbf{c}}_2}$(blue dashdot, right y-axis) under sinusoidal signal from Van's control method.

We can observe from Figure 6 that our proposed adaptive algorithm will increase the gain $\hat{\mathbf{k}}$ when the control performance is not satisfactory and decreases it rapidly when the control performance is good. Thus, $\hat{\mathbf{k}}$ can be regulated timely and precisely based on the current control performance and then lead to good comprehensive performance. For comparisons, the adaptive algorithm (21) used in Van (2018) will always increase the gain $\hat{\mathbf{k}}$ in all situations. When control performance is good, the gain $\hat{\mathbf{k}}$ increases slowly or maintains its value; when the control performance degrades, the gain $\hat{\mathbf{k}}$ will increase rapidly. This will lead to over-large gain $\hat{\mathbf{k}}$ after long-time running and may seriously degrade the control performance.

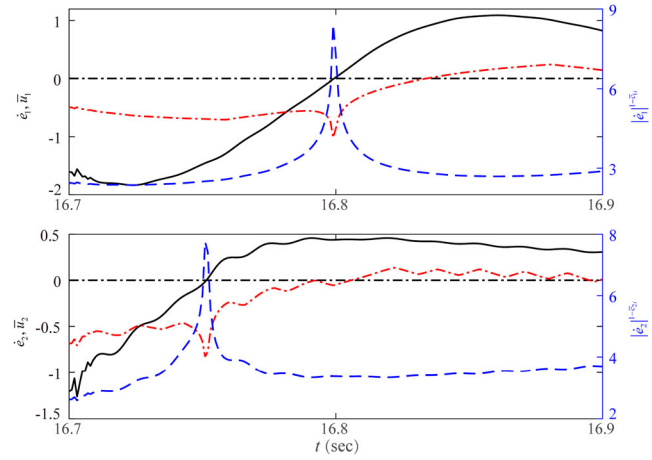

Figure 9. Partial enlarged results of speed tracking error $\dot{\mathbf{e}}$(left y-axis, black solid), control element $\bar{\mathbf{u}}$ (red dashdot, left y-axis) and $|\dot{\mathbf{e}}|^{1-\bar{\mathbf{c}}_2}$(blue dashdot, right y-axis) under sinusoidal signal from Van's control method.

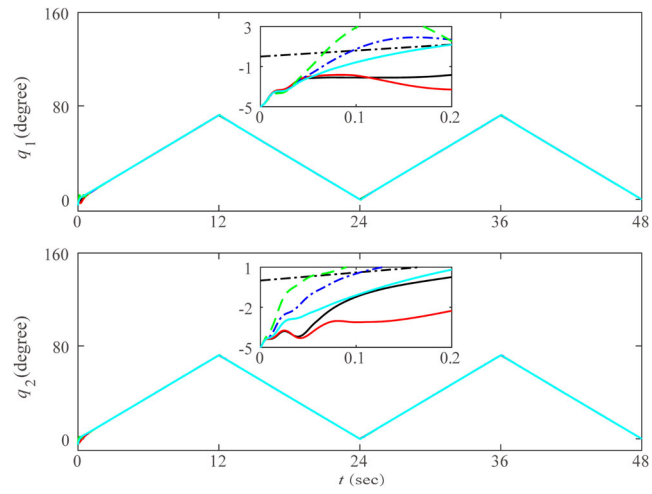

Figure 10. Trajectory tracking performance under triangular wave signal: reference trajectory (black dashdot), our proposed control (black solid), Van's control (red solid), PID 1 (blue dashdot), PID 2 (green dashed) and TDE-based SMC scheme (cyan solid).

Taking Figures 7 and 9 to analyse, we can observe that singularity issue has occurred using Van's method during the simulations. In the steady phase, $\dot{\mathbf{e}}$ fluctuates around $\dot{\mathbf{e}} = 0$ and the element $|\dot{\mathbf{e}}|^{1-\bar{\mathbf{c}}_2}$ has serious fluctuations considering $1 < \bar{c}_{i2} < 2$. This will degrade the control performance or even damage the system hardware under some situations. Moreover, it can be obviously observed from Figure 9 that the control signal $\bar{\mathbf{u}}$ has obvious fluctuation when $\dot{\mathbf{e}}$ cross $\dot{\mathbf{e}} = 0$. This may also degrade the control performance. For comparisons, our proposed control is totally *singularity-free* and, therefore, it can ensure better comprehensive performance.

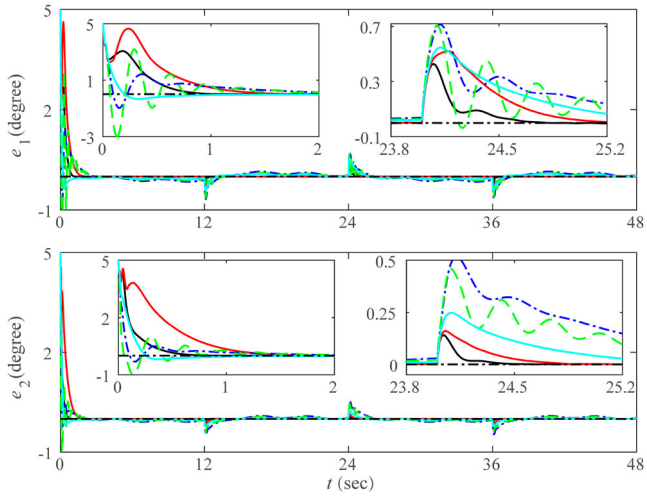

Figure 11. Tracking error under triangular wave signal: our proposed control (black solid), Van's control (red solid), PID 1 (blue dashdot), PID 2 (green dashed) and TDE-based SMC scheme (cyan solid).

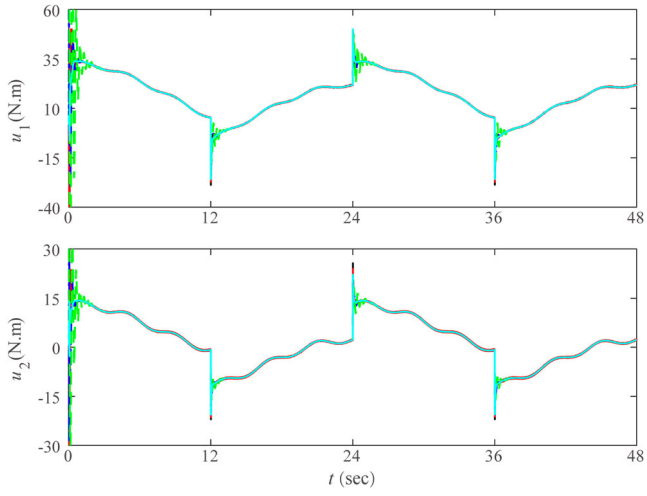

Figure 12. Control efforts under triangular wave signal: our proposed control (black solid), Van's control (red solid), PID 1 (blue dashdot), PID 2 (green dashed) and TDE-based SMC scheme (cyan solid).

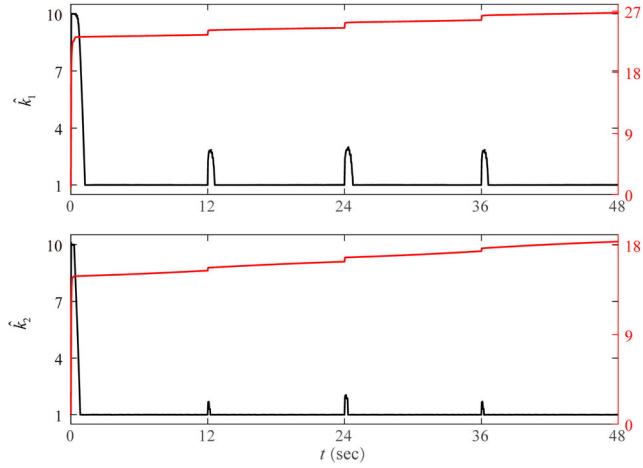

Figure 13. Adaptive gain $\hat{\mathbf{k}}$ under triangular wave signal: our proposed control (black solid), Van's control (red solid), PID 1 (blue dashdot), PID 2 (green dashed) and TDE-based SMC scheme (cyan solid).

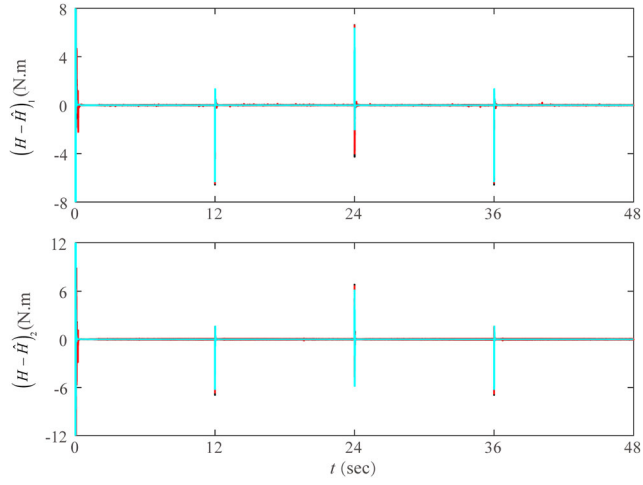

Figure 14. TDE error element ($\mathbf{H} - \hat{\mathbf{H}}$) under triangular wave signal: our proposed control (black solid), Van's control (red solid) and TDE-based SMC scheme (cyan solid).

(2) *Simulation two*: a triangular wave signal is given as the desired trajectory. Then, the control results are given in Figures 10–16.

As shown in Figures 10 and 12, all five controllers can ensure good tracking of the desired trajectory. This verifies the effectiveness of TDE, SM, PID, existing PID-NFTSM and our PID-FONTSM surfaces. Still, our proposed PID-FONTSM surface and corresponding TDE-based control can ensure the best control performance among all five controllers, as indicated in Figure 11. This result effectively demonstrates the advantages of our PID-FONTSM surface and deduced control.

Taking Figures 13 and 14 to analyse, we can see that the over-estimation issue of adaptive gain $\hat{\mathbf{k}}$ also occurs in this case. So is the singularity issue, as shown in Figures 15 and 16.

Generally speaking, our proposed control and other four methods can all provide satisfactory tracking of the desired trajectory thanks to the TDE, SM, PID, existing PID-NFTSM and our PID-FONTSM surfaces. Still, our proposed control shows the best comprehensive performance than the others, which verifies the

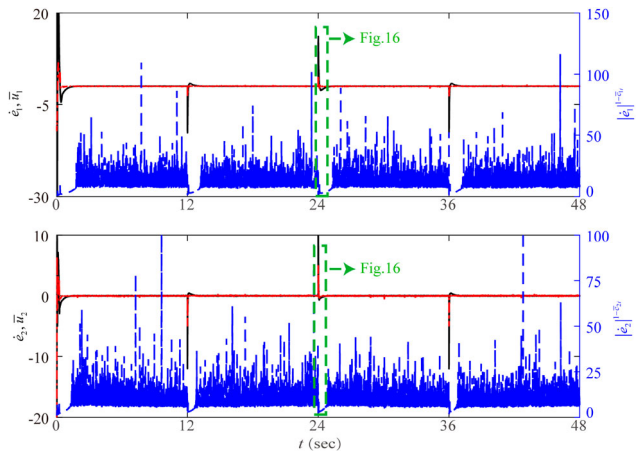

Figure 15. Speed tracking error $\dot{\mathbf{e}}$(left *y*-axis, black solid), control element $\bar{\mathbf{u}}$ (red dashdot, left *y*-axis) and $|\dot{\mathbf{e}}|^{1-\bar{\mathbf{c}}_2}$(blue dashdot, right *y*-axis) under triangular wave signal from Van's control method.

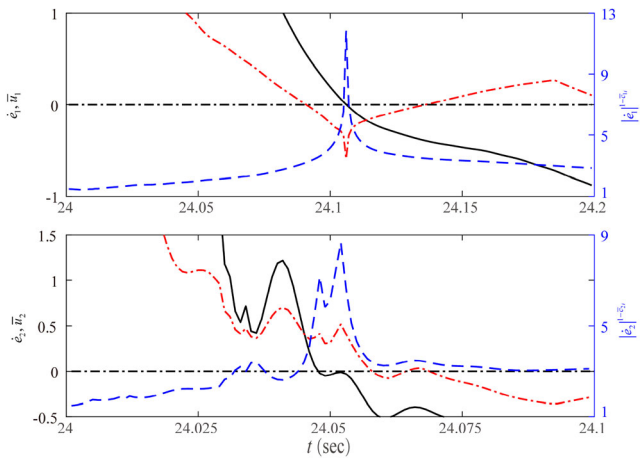

Figure 16. Partial enlarged results of speed tracking error $\dot{\mathbf{e}}$(left *y*-axis, black solid), control element $\bar{\mathbf{u}}$ (red dashdot, left *y*-axis) and $|\dot{\mathbf{e}}|^{1-\bar{\mathbf{c}}_2}$(blue dashdot, right *y*-axis) under triangular wave signal from Van's control method.

advantages of PID-FONTSM surface over the PID-NFTSM surface, PID and SM. The over-estimation of adaptive gain $\hat{\mathbf{k}}$ and singularity issues of Van's control have also been observed in both simulations. For comparisons, our proposed method is free of both issues. In the meanwhile, the two PID controllers present fast convergence and obvious fluctuation in the initial phase due to large gains, and they still provide the largest steady tracking errors than the other three controllers because of relative poor robustness. To conclude, our proposed control method is *model-free*, *accurate* and *singularity-free*.

5. Conclusions

For the high performance control of cable-driven manipulators, a TDE-based adaptive PID-FONTSM control is proposed in this paper. The proposed control utilises TDE to obtain the lumped unknown system dynamics and brings in an effective model-free structure. Then, a PID-FONTSM surface is designed to further enhance the performance. The proposed PID-FONTSM surface utilises a FONTSM surface as its inner loop and a PID-type surface as its outer loop. Thanks to this structure, it can enjoy advantages from both FONTSM and PID dynamics. Afterwards, an adaptive algorithm is designed to timely and precisely regulate the control gain. The proposed control is model-free and easy to use due to TDE; meanwhile, it can ensure high control performance benefitting from the proposed PID-FONTSM surface and adaptive algorithm. The stability of the closed-loop control system under TDE and PID-FONTSM dynamics is analysed based on the Lyapunov stability theory. Finally, comparative simulations demonstrate the effectiveness and advantages of our proposed control method over the existing methods.

Currently, most TDE-based control methods including ours are designed considering only matched disturbance. In the future, the control problem of cable-driven manipulator under mismatched disturbances will be further investigated.

Disclosure statement

No potential conflict of interest was reported by the author(s).

Notes on contributors

Yaoyao Wang (M'17) received the B.S. degree in mechanical engineering from Southeast University, Nanjing, China in 2011 and the Ph.D. degree in mechanical engineering from Zhejiang University, Hangzhou, China in 2016. He is currently an associate professor in the College of Mechanical and Electrical Engineering, Nanjing University of Aeronautics and Astronautics, Nanjing, China. His current research interests include robust control and adaptive control of mechatronic systems; design and control of cable-driven systems, such as cable-driven underwater manipulators and cable-driven flying manipulators.

Jiawei Peng received his B.S. degree in mechanical engineering from College of Mechanical and Electrical Engineering, Nanjing University of Aeronautics and Astronautics, Nanjing, China, in 2019. He is currently working toward the Master degree in the College of Mechanical and Electrical Engineering, Nanjing University of Aeronautics and Astronautics, Nanjing, China. His current research interests include design and control of cable-driven flying manipulators.

Kangwu Zhu received his B.S. degree from Harbin Institute of Technology, Harbin, China, in 2005, M.S. degree from China Ship Scientific Research Center, Wuxi, China, in 2008, and Ph.D. from Zhejiang University, Hangzhou, China, in 2012. He is currently an Associate Researcher with Shanghai Institute of Spaceflight Control Technology, Shanghai, China. His research interests include sliding mode control and nonlinear system control.

Bai Chen received his B.S. and Ph.D. degrees in mechanical engineering from Zhejiang University, Hangzhou, China, in 2000 and 2005, respectively. He is currently a Professor and Ph.D. candidate supervisor at the College of Mechanical and Electrical Engineering, Nanjing University of Aeronautics and Astronautics, Nanjing, China. His current research interests include design and control of surgical robots, cable-driven robots and sperm-like swimming micro robots.

Hongtao Wu received his B.S. degree in mechanical engineering from Northeast Heavy Machinery Institute (the name was changed toYanshan University in 1997), Tsitsihar, China in 1982, M.S., and Ph.D. degrees in mechanical engineering from Tianjin University, Tianjin, China, in 1985 and 1992, respectively. He has been a Professor in Nanjing University of Aeronautics and Astronautics (NUAA) since 1998. He has presided over numbers of the national research project of China. He teaches courses of "Introduction to robotics" and "Computational multibody system dynamics" in NUAA. His research interests include multibody system dynamics, robotics, parallel mechanisms and punching machines.

Funding

This work was supported in part by the National Key R&D Program of China under Grant 2018YFB1309202, Natural Science Foundation of Jiangsu Province (BK20170789), National Natural Science Foundation of China (51705243) and the Open Foundation of the State Key Laboratory of Fluid Power and Mechatronic Systems (GZKF-201915).

ORCID

Yaoyao Wang http://orcid.org/0000-0001-5237-378X

References

Alagoz, B. B., Kavuran, G., Ates, A., & Yeroglu, C. (2017). Reference-shaping adaptive control by using gradient descent optimizers. *Plos One*, *12*(11), Article e0188527. https://doi.org/10.1371/journal.pone.0188527

Babaghasabha, R., Khosravi, M., & Taghirad, H. (2016). Adaptive robust control of fully constrained cable robots: Singular perturbation approach. *Nonlinear Dynamics*, *85*(1), 607–620. https://doi.org/10.1007/s11071-016-2710-8

Baek, J., Cho, S., & Han, S. (2018). Practical time-delay control with adaptive gains for trajectory tracking of robot manipulators. *IEEE Transactions on Industrial Electronics*, *65*(7), 5682–5692. https://doi.org/10.1109/TIE.2017.2782238

Baek, J., Jin, M., & Han, S. (2016). A new adaptive sliding mode control scheme for application to robot manipulators. *IEEE Transactions on Industrial Electronics*, *63*(6), 3628–3637. https://doi.org/10.1109/TIE.2016.2522386

Baek, J., Kwon, W., Kim, B., & Han, S. (2019). A widely-adaptive time-delay control and its application to robot manipulators. *IEEE Transactions on Industrial Electronics*, *66*(7), 5332–5342. https://doi.org/10.1109/TIE.2018.2869347

Chen, Z., Yao, B., & Wang, Q. (2013). Accurate motion control of linear motors with adaptive robust compensation of nonlinear electromagnetic field effect. *IEEE/ASME Transactions on Mechatronics*, *18*(3), 1122–1129. https://doi.org/10.1109/TMECH.2012.2197217

Cui, X., Chen, W., Jin, X., & Agrawal, S. K. (2017). Design of a 7-DOF cable-driven arm exoskeleton (CAREX-7) and a controller for dexterous motion training or assistance. *IEEE/ASME Transactions on Mechatronics*, *22*(1), 161–172. https://doi.org/10.1109/TMECH.2016.2618888

Fei, J., & Lu, C. (2018). Adaptive sliding mode control of dynamic systems using double loop recurrent neural network structure. *IEEE Transactions on Neural Networks and Learning Systems*, *29*(4), 1275–1286. https://doi.org/10.1109/TNNLS.2017.2672998

Gao, R., Zhai, D., & Xie, X. (2020). On the design of output information-based sliding mode controllers for switched descriptor systems: Linear sliding variable approach. *Applied Mathematics and Computation*, *364*, Article 124680. https://doi.org/10.1016/j.amc.2019.124680

Han, Y. (2020). Adaptive output-feedback tracking control for a class of nonlinear systems with input saturation: A multi-dimensional Taylor network-based approach. *International Journal of Systems Science*. https://doi.org/10.1080/00207721.2020.1797226

Han, S., Wang, H., & Tian, Y. (2018). Model-free based adaptive nonsingular fast terminal sliding mode control with time-delay estimation for a 12 DOF multi-functional lower limb

exoskeleton. *Advances in Engineering Software*, *119*, 38–47. https://doi.org/10.1016/j.advengsoft.2018.01.004

Hsia, T. C. (1989). A new technique for robust control of servo systems. *IEEE Transactions on Industrial Electronics*, *36*(1), 1–7. https://doi.org/10.1109/41.20338

Hsia, T. C., Lasky, T. A., & Guo, Z. (1991). Robust independent joint controller design for industrial robot manipulators. *IEEE Transactions on Industrial Electronics*, *38*(1), 21–25. https://doi.org/10.1109/41.103479

Huang, A., & Chen, Y. (2004). Adaptive sliding control for single-link flexible- joint robot with mismatched uncertainties. *IEEE Transactions on Control Systems Technology*, *12*(5), 770–775. https://doi.org/10.1109/TCST.2004.826968

Ibeas, A., & Manuel, S. (2006). Robustly stable adaptive control of a tandem of master–slave robotic manipulators with force reflection by using a multi estimation scheme. *IEEE Transactions on Systems, Man, and Cybernetics, Part B: Cybernetics*, *36*(5), 1162–1179. https://doi.org/10.1109/TSMCB.2006.874693

Ibeas, A., & Manuel, S. (2007). Robust sliding control of robotic manipulators based on a heuristic modification of the sliding gain. *Journal of Intelligent and Robotic Systems*, *48*(4), 485–511. https://doi.org/10.1007/s10846-006-9124-7

Jin, M., Kang, S. H., & Chang, P. H. (2008). Robust compliant motion control of robot with nonlinear friction using time-delay estimation. *IEEE Transactions on Industrial Electronics*, *55*(1), 258–269. https://doi.org/10.1109/TIE.2007.906132

Jin, M., Kang, S. H., Chang, P. H., & Lee, J. (2017). Robust control of robot manipulators using inclusive and enhanced time delay control. *IEEE/ASME Transactions on Mechatronics*, *22*(5), 2141–2152. https://doi.org/10.1109/TMECH.2017.2718108

Jin, M., Lee, J., Chang, P. H., & Choi, C. (2009). Practical nonsingular terminal sliding-mode control of robot manipulators for high-accuracy tracking control. *IEEE Transactions on Industrial Electronics*, *56*(9), 3593–3601. https://doi.org/10.1109/TIE.2009.2024097

Jin, M., Lee, J., & Tsagarakis, N. G. (2017). Model-free robust adaptive control of humanoid robots with flexible joints. *IEEE Transactions on Industrial Electronics*, *64*(2), 1706–1715. https://doi.org/10.1109/TIE.2016.2588461

Kali, Y., Saad, M., & Benjelloun, K. (2018a). Optimal super-twisting algorithm with time delay estimation for robot manipulators based on feedback linearization. *Robotics and Autonomous Systems*, *108*, 87–99. https://doi.org/10.1016/j.robot.2018.07.004

Kali, Y., Saad, M., Benjelloun, K., & Khairallah, C. (2018b). Super-twisting algorithm with time delay estimation for uncertain robot manipulators. *Nonlinear Dynamics*, *93*(2), 557–569. https://doi.org/10.1007/s11071-018-4209-y

Kim, S., & Baek, J. (2017). Force-mode control of rotary series elastic actuators in a lower extremity exoskeleton using model-inverse time delay control. *IEEE/ASME Transactions on Mechatronics*, *22*(3), 1392–1400. https://doi.org/10.1109/TMECH.2017.2687979

Kim, J., Chang, P. H., & Jin, M. (2017). Fuzzy PID controller design using time-delay estimation. *Transactions of the Institute of Measurement and Control*, *39*(9), 1329–1338. https://doi.org/10.1177/0142331216634833

Kim, J., Joe, H., Yu, S., Lee, J., & Kim, M. (2016). Time-delay controller design for position control of autonomous underwater vehicle under disturbances. *IEEE Transactions on Industrial Electronics*, *63*(2), 1052–1061. https://doi.org/10.1109/TIE.2015.2477270

Korayem, M. H., Yousefzadeh, M., & Manteghi, S. (2017). Dynamics and input–output feedback linearization control of a wheeled mobile cable-driven parallel robot. *Multibody System Dynamics*, *40*(1), 55–73. https://doi.org/10.1007/s11044-016-9543-6

Lakhekar, G. V., & Waghmare, L. M. (2018). Adaptive fuzzy exponential terminal sliding mode controller design for nonlinear trajectory tracking control of autonomous underwater vehicle. *International Journal of Dynamics and Control*, *6*(4), 1690–1705. https://doi.org/10.1007/s40435-017-0387-6

Li, M., & Chen, Y. (2019). Robust adaptive sliding mode control for switched networked control systems with disturbance and faults. *IEEE Transactions on Industrial Informatics*, *15*(1), 193–204. https://doi.org/10.1109/TII.2018.2808921

Li, J., & Yang, G. H. (2020). Fuzzy descriptor sliding mode observer design: A canonical form-based method. *IEEE Transactions on Fuzzy Systems*. https://doi.org/10.1109/TFUZZ.2019.2930036

Li, J., & Zhang, Q. (2019). Fuzzy reduced-order compensator-based stabilization for interconnected descriptor systems via integral sliding modes. *IEEE Transactions on systems, Man, and Cybernetics: Systems*, *49*(4), 752–765. https://doi.org/10.1109/TSMC.2017.2707499.

Liu, X., Yang, C., Chen, Z., Wang, M., & Su, C. (2018). Neuro-adaptive observer based control of flexible joint robot. *Neurocomputing*, *275*, 73–82. https://doi.org/10.1016/j.neucom.2017.05.011

Lochan, K., Singh, J. P., Roy, B. K., & Subudhi, B. (2020). Adaptive global super-twisting sliding mode control-based filter for trajectory synchronisation of two-link flexible manipulators. *International Journal of Systems Science*. https://doi.org/10.1080/00207721.2020.1795947

Ma, H., Li, Y., & Xiong, Z. (2019). Discrete-time sliding-mode control with enhanced power reaching law. *IEEE Transactions on Industrial Electronics*, *66*(6), 4629–4638. https://doi.org/10.1109/TIE.2018.2864712

Roy, S., & Kar, I. N. (2017). Adaptive sliding mode control of a class of nonlinear systems with artificial delay. *Journal of the Franklin Institute*, *354*(18), 8156–8179. https://doi.org/10.1016/j.jfranklin.2017.10.010

Roy, S., Kar, I. N., Lee, J., & Jin, M. (2017). Adaptive robust time-delay control for a class of uncertain Euler-Lagrange systems. *IEEE Transactions on Industrial Electronics*, *64*(9), 7109–7119. https://doi.org/10.1109/TIE.2017.2688959

Shang, W., Zhang, B. Y., Zhang, B., Zhang, F., & Cong, S. (2019). Synchronization control in the cable space for cable-driven parallel robots. *IEEE Transactions on Industrial Electronics*, *66*(6), 4544–4554. https://doi.org/10.1109/TIE.2018.2864512

Tepljakov, A., Alagoz, B. B., Gonzalez, E., Petlenkov, E., & Yeroglu, C. (2018). Model reference adaptive control scheme for retuning method-based fractional-order PID control with disturbance rejection applied to closed-loop control of a magnetic levitation system. *Journal of Circuits, Systems and Computers*, *27*(11), Article 1850176. https://doi.org/10.1142/S0218126618501761

Townsend, W. T. (1988). *The effect of transmission design on force- controlled manipulator performance* [Doctoral dissertation]. Massachusetts Institute of Technology. http://dspace.mit.edu/handle/1721.1/6835

Tran, D. T., Ba, D. X., & Ahn, K. K. (2020). Adaptive backstepping sliding mode control for equilibrium position tracking of an electrohydraulic elastic manipulator. *IEEE Transactions on Industrial Electronics*, *67*(5), 3860–3869. https://doi.org/10.1109/TIE.2019.2918475

Utkin, V. (1993). Sliding mode control design principles and applications to electric drives. *IEEE Transactions on Industrial Electronics*, *40*(1), 23–36. https://doi.org/10.1109/41.184818

Van, M. (2018). An enhanced robust fault tolerant control based on an adaptive fuzzy PID-nonsingular fast terminal sliding mode control for uncertain nonlinear systems. *IEEE/ASME Transactions on Mechatronics*, *23*(3), 1362–1371. https://doi.org/10.1109/TMECH.2018.2812244

Wang, Y., Chen, J., Yan, F., Zhu, K., & Chen, B. (2019). Adaptive super-twisting fractional-order nonsingular terminal sliding mode control of cable-driven manipulators. *ISA Transactions*, *86*, 163–180. https://doi.org/10.1016/j.isatra.2018.11.009

Wang, Y., Gu, L., Xu, Y., & Cao, X. (2016). Practical tracking control of robot manipulators with continuous fractional-order nonsingular terminal sliding mode. *IEEE Transactions on Industrial Electronics*, *63*(10), 6194–6204. https://doi.org/10.1109/TIE.2016.2569454

Wang, Y., Li, S., Wang, D., Ju, F., Chen, B., & Wu, H. (2020). Adaptive time-delay control for cable-driven manipulators with enhanced nonsingular fast terminal sliding mode. *IEEE Transactions on Industrial Electronics*. https://doi.org/10.1109/TIE.2020.2975473

Wang, Y., Li, B., Yan, F., & Chen, B. (2019). Practical adaptive fractional-order nonsingular terminal sliding mode control for a cable-driven manipulator. *International Journal of Robust and Nonlinear Control*, *29*(5), 1396–1417. https://doi.org/10.1002/rnc.4441

Wang, Y., Liu, L., Chen, J., Ju, F., Chen, B., & Wu, H. (2020). Practical robust control of cable-driven robots with feedforward compensation. *Advances in Engineering Software*, *145*, Article 102801. https://doi.org/10.1016/j.advengsoft.2020.102801

Wang, Y., Liu, L., Wang, D., Ju, F., & Chen, B. (2020). Time-delay control using a novel nonlinear adaptive law for accurate trajectory tracking of cable-driven robots. *IEEE Transactions on Industrial Informatics*, *16*(8), 5234–5243. https://doi.org/10.1109/TII.2019.2951741

Wang, Y., Yan, F., Chen, J., Ju, F., & Chen, B. (2019). A new adaptive time-delay control scheme for cable-driven manipulators. *IEEE Transactions on Industrial Informatics*, *15*(6), 3469–3481. https://doi.org/10.1109/TII.2018.2876605

Wang, Y., Yan, F., Jiang, S., & Chen, B. (2018). Time delay control of cable-driven manipulators with adaptive fractional-order nonsingular terminal sliding mode. *Advances in Engineering Software*, *121*, 13–25. https://doi.org/10.1016/j.advengsoft.2018.03.004

Wang, Y., Yan, F., Jiang, S., & Chen, B. (2020). Adaptive nonsingular terminal sliding mode control of cable-driven manipulators with time delay estimation. *International Journal of Systems Science*, *51*(8), 1429–1447. https://doi.org/10.1080/00207721.2020.1764659

Wang, Y., Yan, F., Zhu, K., Chen, B., & Wu, H. (2019). A new practical robust control of cable-driven manipulators using time- delay estimation. *International Journal of Robust and Nonlinear Control*, *29*(11), 3405–3425. https://doi.org/10.1002/rnc.4566

Wang, Y., Zhu, K., Chen, B., & Jin, M. (2020). Model-free continuous nonsingular fast terminal sliding mode control for cable-driven manipulators. *ISA Transactions*, *98*, 483–495. https://doi.org/10.1016/j.isatra.2019.08.046

Xu, W., Liu, T., & Li, Y. (2018). Kinematics, dynamics, and control of a cable-driven hyper-redundant manipulator. *IEEE/ASME Transactions on Mechatronics*, *23*(4), 1693–1704. https://doi.org/10.1109/TMECH.2018.2842141

Yagmur, N., & Alagoz, B. B. (2019, September 21–22). *Adaptive gradient descent control of stable, first order, time-delay dynamic systems according to time-varying FIR filter model assumption*. 2019 International Artificial Intelligence and Data Processing Symposium (IDAP), Malatya, Turkey.

Yu, S., Yu, X., Shirinzadeh, B., & Man, Z. (2005). Continuous finite-time control for robotic manipulators with terminal sliding mode. *Automatica*, *41*(11), 1957–1964. https://doi.org/10.1016/j.automatica.2005.07.001

Appendix

The same analysis procedures from Jin et al. (2009) and Kali et al. (2018b) are used to prove the boundedness of $\boldsymbol{\varepsilon}$ and $\dot{\boldsymbol{\varepsilon}}$. Before giving the proof, the following property is necessary.

Property A.1 ((Kali et al., 2018b).): The inertia matrix $\mathbf{M}(\mathbf{q})$ given in (2) is positive definite symmetrical and bounded, and it fulfils the following inequality:

$$0 < M_1 \leq ||\mathbf{M}(\mathbf{q})|| \leq M_2 < \infty \tag{A1}$$

where M_1 and M_2 are two known positive constants.

Substituting the control (14)–(16) into dynamics (4) yields

$$\boldsymbol{\varepsilon} = \mathbf{u} - \ddot{\mathbf{q}} \tag{A2}$$

Combining (A2) and (14)–(16), we have

$$\begin{aligned}\mathbf{M}\boldsymbol{\varepsilon} &= \mathbf{M}(\mathbf{u} - \ddot{\mathbf{q}}) \\ &= \mathbf{M}\mathbf{u} + \mathbf{C}(\mathbf{q}, \dot{\mathbf{q}})\dot{\mathbf{q}} + \mathbf{G}(\mathbf{q}) + \mathbf{F}(\mathbf{q}, \dot{\mathbf{q}}) + \boldsymbol{\tau}_d\end{aligned}$$

$$+ \mathbf{J}\ddot{\boldsymbol{\theta}} + \mathbf{D}_m\dot{\boldsymbol{\theta}} - \bar{\mathbf{M}}\mathbf{u} - \mathbf{H}(t-L) \tag{A3}$$

Considering (5), we have the following equation as

$$\begin{aligned}\mathbf{H}(t-L) = {} & (\mathbf{M}-\bar{\mathbf{M}})(t-L)\ddot{\mathbf{q}}(t-L) \\ & + [\mathbf{C}\dot{\mathbf{q}}](t-L) + \mathbf{G}(t-L) \\ & + \mathbf{F}(t-L) + [\mathbf{J}\ddot{\boldsymbol{\theta}}](t-L) \\ & + [\mathbf{D}_m\dot{\boldsymbol{\theta}}](t-L) + \boldsymbol{\tau}_d(t-L)\end{aligned} \tag{A4}$$

Substituting (A4) into (A3), we have

$$\mathbf{M}\boldsymbol{\varepsilon} = (\mathbf{M}-\bar{\mathbf{M}})\mathbf{u} - [\mathbf{M}(t-L) - \bar{\mathbf{M}}]\ddot{\mathbf{q}}(t-L) + \Delta \tag{A5}$$

where $\Delta = \Theta - \Theta(t-L), \Theta = \mathbf{C}\dot{\mathbf{q}} + \mathbf{G} + \mathbf{F} + \mathbf{J}\ddot{\boldsymbol{\theta}} + \mathbf{D}_m\dot{\boldsymbol{\theta}} + \boldsymbol{\tau}_d$. For sufficiently small L, the Δ is obvious bounded (Jin et al., 2009). According to (A2), we have $\ddot{\mathbf{q}}(t-L) = \mathbf{u}(t-L) - \boldsymbol{\varepsilon}(t-L)$. Then, (A5) can be further written as

$$\begin{aligned}\mathbf{M}\boldsymbol{\varepsilon} &= (\mathbf{M}-\bar{\mathbf{M}})\mathbf{u} - (\mathbf{M}-\bar{\mathbf{M}})\ddot{\mathbf{q}}(t-L) \\ &\quad + [\mathbf{M}-\mathbf{M}(t-L)]\ddot{\mathbf{q}}(t-L) + \Delta \\ &= (\mathbf{M}-\bar{\mathbf{M}})\mathbf{u} - (\mathbf{M}-\bar{\mathbf{M}})[\mathbf{u}(t-L) - \boldsymbol{\varepsilon}(t-L)] \\ &\quad + [\mathbf{M}-\mathbf{M}(t-L)]\ddot{\mathbf{q}}(t-L) + \Delta \\ &= (\mathbf{M}-\bar{\mathbf{M}})\boldsymbol{\varepsilon}(t-L) + (\mathbf{M}-\bar{\mathbf{M}})[\mathbf{u} - \mathbf{u}(t-L)] \\ &\quad + [\mathbf{M}-\mathbf{M}(t-L)]\ddot{\mathbf{q}}(t-L) + \Delta\end{aligned} \tag{A6}$$

Afterwards, (A6) can be re-organised as

$$\boldsymbol{\varepsilon} = \mathbf{E}\boldsymbol{\varepsilon}(t-L) + \mathbf{E}\xi_1 + \xi_2 \tag{A7}$$

where $\xi_1 = \mathbf{u} - \mathbf{u}(t-L), \xi_2 = \mathbf{M}^{-1}([\mathbf{M} - \mathbf{M}(t-L)]\ddot{\mathbf{q}}(t-L) + \Delta)$ and $\mathbf{E} = \mathbf{I} - \mathbf{M}^{-1}\bar{\mathbf{M}}$. When the time delay L is sufficiently small, the element ξ_1 and ξ_2 are bounded. Meanwhile, the condition $||\mathbf{E}|| < 1$ can be easily fulfilled with proper selection of $\bar{\mathbf{M}}$.

The (A7) can be re-written in the discrete form as

$$\boldsymbol{\varepsilon}(k) = \mathbf{E}(k)\boldsymbol{\varepsilon}(k-1) + \mathbf{E}(k)\xi_1(k) + \xi_2(k) \tag{A8}$$

Considering $||\mathbf{E}|| < 1$, (A8) will be asymptotically bounded under bounded forcing input ξ_1 and ξ_2. Therefore, the TDE error $\boldsymbol{\epsilon}$ will be bounded. Furthermore, the $\dot{\boldsymbol{\varepsilon}}$ can be given as

$$\begin{aligned}\dot{\boldsymbol{\varepsilon}}(t) &= \frac{1}{L}[\boldsymbol{\varepsilon}(t) - \boldsymbol{\varepsilon}(t-L)] \\ &= \frac{1}{L}(\mathbf{E}-\mathbf{I})\boldsymbol{\varepsilon}(t-L) + \frac{1}{L}[\mathbf{E}\xi_1 + \xi_2] \\ &= \frac{1}{L}(-\mathbf{M}^{-1}\bar{\mathbf{M}})\boldsymbol{\varepsilon}(t-L) + \frac{1}{L}[\mathbf{E}\xi_1 + \xi_2]\end{aligned} \tag{A9}$$

Then, we have

$$||\dot{\boldsymbol{\varepsilon}}(t)|| = \frac{1}{L}||(-\mathbf{M}^{-1}\bar{\mathbf{M}})\boldsymbol{\varepsilon}(t-L) + \mathbf{E}\xi_1 + \xi_2|| \tag{A10}$$

Using the **Property A1** (A1), i.e. $||\mathbf{M}^{-1}|| \leq \frac{1}{M_1}$, we have

$$||\dot{\boldsymbol{\varepsilon}}(t)|| \leq \frac{1}{L}\left(\frac{Sup(\bar{m}_{ii})_{i=1:n}}{M_1}||\boldsymbol{\varepsilon}(t-L)|| + ||\mathbf{E}\xi_1 + \xi_2||\right) \leq \Omega \tag{A11}$$

Thus, the derivative of TDE error $\boldsymbol{\epsilon}$, *i.e.*$\dot{\boldsymbol{\varepsilon}}$, is bounded.